



Sedapp: a non-linear diffusion-based forward stratigraphic model for shallow marine environments

Jingzhe Li^{1,2}, Piyang Liu³, Shuyu Sun⁴ (✉), Zhifeng Sun^{2,1}, Yongzhang Zhou⁵, Liang Gong⁶, Jinliang Zhang⁷, Dongxing Du^{1,2}

5

1. College of Electromechanics, Qingdao University of Science and Technology, Qingdao 266061, China
2. Geo-Energy Research Institute, Qingdao University of Science and Technology, Qingdao 266061, China
3. School of Science, Qingdao University of Technology, Qingdao, 266520, China
4. King Abdullah University of Science and Technology, Jeddah 23955-6900, Saudi Arabia
- 10 5. School of Earth Science and Geological Engineering, Sun Yat-sen University, Guangzhou 510275, China
6. School of New Energies, China University of Petroleum (EastChina), Qingdao 266555, China
7. Department of Geography, Beijing Normal University, Beijing 100875, China

Correspondence to: Shuyu Sun (frank.sun.sa@gmail.com)

Abstract

15 The formation of stratigraphy in shallow marine environments has long been an important topic within the geologic community. Although many advances have been made in the field of forward stratigraphic modelling (FSM), there are still some shortcomings to the existing models. In this work, the authors present our recent development and application of Sedapp: a new non-linear open-source R code for FSM. This code uses an integrated depth-distance related function as the expression of the
20 transport coefficient to underpin the FSM with more along-shore details. In addition to conventional parameters, a negative-feedback sediment supply rate and a differentiated deposition-erosion ratio were also introduced. All parameters were implemented in a non-linear manner. Sedapp is a 3D (2DH) tool while also capable of 2D (1DH) scenarios. Two simplified case studies were conducted. The results show that Sedapp can not only assist in geologic interpretation, but is also an efficient tool for internal
25 architecture predictions.

Keywords: Forward stratigraphic modelling, continental shelf, R codes, fluvial-deltaic, continental fault basin



1 Introduction

Shallow marine areas are among the most active environments for sedimentation, where sea level, tectonism, climate all influence the interactions between land and sea. Stratigraphic formation in this environment has long been an important topic within the geoscience community, which has directly resulted in the emergence of sequence stratigraphy (Haq et al., 1987; Li et al., 2015; Catuneanu, 2019). Traditional qualitative methods on this subject have made great advances in the past half century, but it is difficult to test the validity and internal consistency of a new concept and are less likely to raise counter-intuitive ideas which may actually be true (Burgess, 2012; Burgess and Prince, 2015).

Computer modelling can help resolve this problem. The methodology is usually called forward stratigraphic modelling (FSM) (Griffiths and Hadler-Jacobsen, 1995; Dalman and Weltje, 2012; Sangster et al., 2019), although it was also called stratigraphic forward modelling (Burgess, 2006; Sacchi et al., 2015; 2016; Ding et al., 2019), basin filling modelling (Syvitski and Hutton, 2001; Hutton and Syvitski, 2008; Li et al., 2020), and stratigraphic simulation (Rivenaes, 1992; 1997; Lawrence et al., 1990), etc.

FSM deals mainly with long-term geomorphologic/stratigraphic dynamics (Paola, 2000). It is slightly different from sediment fluid-flow models, which deal more with the fluid-flow dynamics by solving modified Navier-Stokes equations within a full study domain (generally shallow water equations, e.g. HydroSedFoam of Zhu et al., 2019 or Delft3D in Ramos et al., 2019). FSM models can be classified into two types, i.e. rule-based models (based on geometric or fuzzy logic) and equation-based models (Paola, 2000; Syvitski and Hutton, 2001; Burgess et al., 2012; Sacchi et al., 2015). The first type easily captures essential features and is less time-intensive, while it does a relatively poor job of demonstrating predictability and revealing the physical processes (Strobel et al., 1989; Kendall et al., 1991; Burgess, 2012). The latter type is also known as deductive models, which are process-based and solve governing equations (Kaufman et al., 1991; Rivenaes, 1992; Granjeon and Joseph, 1999; Griffiths et al., 2001; Hutton and Syvitski, 2008; Li et al., 2020). For these long-term processes, sediment flux is usually assumed to be proportional to the topographic gradient. Thus, a diffusion equation like Eq. (1) is generally used to derive the governing equations in FSM models (Salles et al., 2018; Ding et al., 2019).



$$\frac{\partial h}{\partial t} = \nabla \cdot (\Gamma \nabla h) \quad (1)$$

where h denotes the topography, t denotes the time and Γ denotes the transport coefficient.

Diffusion-based models are good at modeling scaled stratigraphic sequence (relative larger scales, e.g. clinoform formation) processes. Γ in Eq. (1) can be defined using different values for different environments (Zhang et al., 2020). Various Γ types are used based on different needs and environments (Rivenaes, 1997; Zhang et al., 2020). Models with constant Γ values are usually called linear models; otherwise, they are known as non-linear models.

Although the sediment diffusion assumption is considered a practical representation of long-term slope processes, it is still too simplistic when the Γ is used as a constant because natural agents such as air and water, phenomena such as mass wasting, and biological agents actually move sediment at rates that are not determined solely by slope (Salles et al., 2018). This severely limits the application scope of linear diffusion-based models. On the contrary, non-linear models are relatively more flexible. Many non-linear models define the transport coefficient using water depth-related functions (e.g., Clarke et al. 1983; Kaufman, 1991). These water depth models work well in general coastal zones. However, in the shallow marine environments with river injection, the water depth models are usually not applicable. Depositional processes around the river mouth are more active than those at a distance, even when they are at the same water depth. Hence, it is difficult for water depth models to reveal along-shore variability, especially in 3D scenarios (actually 2D-H, with two horizontal dimensions and the elevation H). Because of this reason, many hybrid hydrodynamic-diffusion models were proposed. For example, river plume was introduced to differentiate the suspended sediment fluxes along the coastline (Syvitski and Hutton, 2001; Hutton and Syvitski, 2008; Dalman and Weltje., 2012). This treatment realized the modelling of the convex shapes of delta out from the river mouths. However, the computational load was also significantly increased because of the newly added advection-diffusion process. The introduction of many hydrodynamic parameters also increased the difficulty of its usage.

In addition, many existing models are not free or open-source, making it difficult for people to reproduce and improve them. Some codes, although free, can only be used in Linux systems, which makes them inconvenient to use in most PC terminals.

In this paper, we propose a new non-linear model, which is expected to overcome the shortcomings of the existing models. Along with some other features, this model is integrated into a



85 framework called Sedapp, which is an open-source and cross-platform application written in R. We use
 examples to show how this model works and test its effectiveness and convenience in reconstruction of
 sedimentary systems, revealing their internal architectures.

2 Methodology

2.1 Mathematical model

90 The Sedapp mathematical model can be expressed as follows:

$$F_i \frac{\partial h}{\partial t} = \max\left(\nabla \cdot (\Gamma_i \nabla h), \frac{1}{Der} \nabla \cdot (\Gamma_i \nabla h)\right) + q \quad (2)$$

$$\sum_i^n F_i = 1 \quad (3)$$

where F_i is the fraction of the i th class of lithology, h is elevation, t is time, ∇ is the nabla operator,
 Der is a user-defined parameter denoting the ratio of deposition to erosion (it can be a scalar, vector or
 95 tensor value depending on its temporal and spatial variability), Γ_i is the diffusion coefficient for the i th
 class of lithology, and q is the source term that is a function of coordinates and time (the source term is
 used only for endogenetic sedimentation, especially carbonates. If endogenetic sedimentation is
 ignored, the source term can be left out). Among them, h and F_i are the primary unknowns.

Note that Γ_i cannot be outside the parentheses, because they are not constants but rather functions
 100 of spatial coordinates and time. The expression of a general Γ can be expressed as:

$$\Gamma = \max\left(\alpha e^{-\frac{D(x,t)^\eta}{\beta}}, \alpha_{wd} e^{-\frac{Wd(x,t)^{\eta_{wd}}}{\beta_{wd}}}\right) + \varepsilon \quad (4)$$

where α/α_{wd} are preexponential factors (L^2/T), η/η_{wd} are distance indexes (no dimension), β/β_{wd} are
 spatial scale factors (L^η or $L^{\eta_{wd}}$), and ε is an adjustment factor (L^2/T) reflecting the environment
 energy. In particular, distance function $D=D(x,t)$ and water depth function $Wd(x,t)$ change with spatial
 105 coordinates and time, and they work for the marine portion only.

When $Der = 1$ and $n = 2$, the 3D (actually 2DH, because h is another dimension perpendicular to
 x and y) scenario for Eq. (2) and Eq. (3) can also be expressed as:

$$F \frac{\partial h}{\partial t} = \frac{\partial}{\partial x} \left(\Gamma_1 \frac{\partial h}{\partial x} \right) + \frac{\partial}{\partial y} \left(\Gamma_1 \frac{\partial h}{\partial y} \right) + q(x, y, t) \quad (5)$$



$$(1-F)\frac{\partial h}{\partial t} = \frac{\partial}{\partial x}\left(\Gamma_2 \frac{\partial h}{\partial x}\right) + \frac{\partial}{\partial y}\left(\Gamma_2 \frac{\partial h}{\partial y}\right) + q(x, y, t) \quad (6)$$

110 where x and y are spatial coordinates. This is especially suitable for cases dealing only with two classes
of lithology for simplicity, where Γ_1 is the transport coefficient for sand and Γ_2 is the transport
coefficient for mud.

For 2D (1D-H) scenarios, especially along the section line through the river mouth, the distance
related term is generally larger than the water depth related term, so the latter term within the max
115 function in Eq. (4) is usually omitted. For convenience in coding, also ignoring the endogenetic
sedimentation, Eq. (5), Eq. (6) and Eq. (4) can be simplified into:

$$F \frac{\partial h}{\partial t} = \frac{\partial}{\partial x}\left(\Gamma_1 \frac{\partial h}{\partial x}\right) \quad (7)$$

$$(1-F)\frac{\partial h}{\partial t} = \frac{\partial}{\partial x}\left(\Gamma_2 \frac{\partial h}{\partial x}\right) \quad (8)$$

$$\Gamma_i = \alpha_i \cdot e^{-\frac{(c \cdot D(x,t))^2}{E}} + \varepsilon, i = 1,2 \quad (9)$$

120 The joint effect of c and E in Eq. (9) is equivalent to that of β in Eq. (4). The variable c here, with
a dimension of L^{-1} , is mainly used to facilitate the scale of distance and differentiate the transport
characteristics of different sediment types (e.g., sand and mud). E is a dimensionless constant that
represents hydraulic characteristic energy.

2.2 Code Implementation

125 Sedapp was written in the R language and its solution procedure was based on the finite volume
method (FVM), which has the desired property of local mass conservation and has a clear physical
meaning (Versteeg and Malalasekera, 2007; Moukalled et al., 2016; Liu P. et al., 2017). The
cell-centered variable arrangement method was used to store the unknowns at the grid element
centroids. The non-linearity was implemented through stepwise iteration (Fig.1).

130 The brief work-flow within a single time step is as below:

- 1) Implement user-defined tectonic subsidence and update the topography;
- 2) Implement user-defined sea level and identify/update the shoreline location;
- 3) Solve the differential deposition/erosion function;
- 4) Implement the compaction and isostatic subsidence.



135 Step 3) is a major step. According to the hypothesis of diffusion-based FSM models, the change
rate (by either deposition or erosion) is proportional to the gradient of the slope (Fernandes et al., 1997;
Pelletier, 2013). If we use the diffusion equation/law directly without any differential treatments
between deposition and erosion (in other words, Der is held at 1), it will be contrary to the geological
knowledge that deposition and erosion processes are two distinct processes with different rates. Hence,
140 the $\max()$ function is used as in Eq. (2). Generally, the erosion process occurs at a different rate than
deposition (also called erosion constraints, see Galy and France-Lanord, 2001), so Der is usually not
equal to 1. For example, if we wanted the erosion rate to be only 1/100 of the deposition rate, the Der
can be set to 100. In this case, if it is a deposition process (namely the $\frac{\partial h}{\partial t} > 0$), $\nabla \cdot (\Gamma_i \nabla h)$ would be
larger than $\frac{1}{der} \nabla \cdot (\Gamma_i \nabla h)$, and $\nabla \cdot (\Gamma_i \nabla h)$ is used. Otherwise, the $\frac{1}{der} \nabla \cdot (\Gamma_i \nabla h)$ is used. If a
145 non-erosion case is desired, Der can be set to a very large value.

Generally, sediment supply rate cannot be directly defined through boundary condition settings,
since the latter can only determine the boundary slope. Therefore, Sedapp uses a negative-feedback
strategy to define the sediment supply rate. At each time step, the total amount of deposition within a
step is first calculated using the previously defined α_{test} , and then the adjusted α_{mod} is calculated by
150 Eq. (10):

$$\alpha_{mod} = \alpha_{test} \frac{V_{expected}}{V_{test}} \quad (10)$$

where α_{mod} denotes the modified α of this time step; $V_{expected}$ denotes the expected sediment increment,
namely the sediment supply rate; and V_{test} denotes the computed sediment increment with α_{test} .

3 Characteristics

155 3.1 Nonlinear transport coefficients

The nonlinear transport coefficient is a feature of Sedapp. Sedapp's transport coefficient uses a
function of both the distance from the estuary and the water depth. This feature makes it easier to
simulate fluvial-deltaic processes in 3D scenarios, which can reflect changes along the shore. Even in
2D cases, this feature also has some advantages (see the discussion section for details).

160 Generally, a smaller c value results in higher sediment travel distance and a larger distribution



range when the total amount of sediment is fixed. For example, the c of mud is usually set to 50%-85% of sand, thus reflecting the differential deposition of sand and mud. In addition, the environment energy \mathcal{E} can also influence the sediment travel distance that a larger \mathcal{E} can make the sediment travel further. As sedimentation progresses, the position of the estuary may change, so the distance from the estuary is updated at each time step to achieve the nonlinearity of Γ .

3.2 Differential and customizable deposition/erosion rate

During the actual deposition process, the properties of the lower strata (such as compaction degree, lithology, and age, etc.), as well as some external environmental factors (such as temperature, humidity and pH value, etc.), will affect the erosion rate. Therefore, the customized treatment of erosion rate is another Sedapp characteristic.

In Sedapp, the deposition rate is a parameter that can be specified directly (for the adjustment process see section 2.2). Furthermore, the Der parameter is a user-defined parameter that controls the ratio of deposition rate to erosion rate. When Der is 1, the deposition rate is equal to the denudation rate (Fig.2a), and when Der value is 10 or 100, denudation is significantly weakened (Fig.2b). Theoretically, if the value of Der is large enough, it is equivalent to completely eliminating the denudation effect. Der values should be customized according to the actual situation.

3.3 Customizable compaction

Compaction is an important geological process after sediment deposition, especially when the sediment thickness is very high. In Sedapp, the compaction process can be easily realized by setting the composition of lithology and porosity curves.

In this paper, we designed a pyramid-shaped mountain simulation commonly used by other researchers (as shown in Fig.3, see Rivenaes,1992 and Yuan et al.,2019 for reference). The Der value was set to 1. The sediment supply ratio of sand and mud was set to 1:1, and the porosity curve was set as shown in Fig.3d. After simulation, the top of the pyramid was denuded and the foot of the pyramid had deposited sediment of a given thickness.

To illustrate the effect of compaction, Sedapp introduces a scale factor that can enlarge the longitudinal scale. Fig.3a shows the original compression scale (that is, the scale factor was equal to 1), and the scale factors in Fig.3b and Fig.3c were 100 and 1000, respectively. It can be seen that sediment



thickness at the foot of the pyramid in Fig.3c was significantly smaller than that in Fig.3a. The factors
190 that caused these differences were not only depth but also the proportion of sand and mudstone and the
shape of depth-porosity curves, which can be easily adapted to different scenarios by modifying the
lithologic proportion and porosity-depth functions in Sedapp.

4 Verification of Sedapp

To identify how well the algorithm works within geological context, some simple benchmark
195 simulations are given below.

4.1 Typical stacking patterns

Typical stacking patterns including forced regression, normal regression, and transgression can
be formed (Fig.4) by fixing sediment supply while controlling the adjusted sea level rise rate.

During the period of sea-level decline, the shoreline moved seaward, and the onlap points also
200 moved seaward and form the offlap and downlap stratigraphic termination structures (Fig.4a). During
slow sea-level rise, the shoreline continued to move seaward, but the onlap points started to move
landward, forming an onlap termination structure. At the other end, the downlap structure continued to
exist. During rapid sea-level rise, the shoreline started to move landward and the onlap points also
moved landward. At this time, downlap structure did not exist above the slope break, but may have
205 existed below the slope break.

4.2 Typical two-cycle scenario

To demonstrate the complete base level changing process, this paper designed a simulation with
two full sinusoidal cycles as shown in Fig.5. In the first cycle, the shoreline dropped and moved
seaward. Then it slowly rose and gradually moved landward until it reached the highest point and
210 tended to stabilize. The water depth of deposition in the strata gradually deepened from left to right on
the marine side (Fig.5a), and the sandy content reached a maximum around the shoreline (Fig.5b) near
the shoreline. In the strata on the land side, the sand content was stratified. The sand content was
relatively large during the early transgression and subsequently relatively small. The second cycle was
located above the first cycle and continued the same characteristics as the first cycle, but the deposition
215 range was enlarged and the average single layer thickness was thinner.



4.3 Case studies

1) Model 1

In order to better display the 3D performance of Sedapp, this paper designed a model called
220 Model 1. Its length and width ranges were both 200m, and the elevation range was about 10m. The
mesh was 200×200 in x-y plane. The time span of the model was set at 10 Ma, and the step size was
set at 0.5 Ma. Sea level was kept constant at 3 m. Its initial topography was set as that in Fig.6a. A river
was set up in the central position of y-axis ($y = 100\text{m}$). The channel shape of the river was set in
advance being a sine curve. Fluvial profile slope is set to a constant of 0.00357, while the sediment
225 supply rate was not defined since it could vary according to the fluvial profile slope. The other main
parameters of the model are shown in Tab. 1.

The projection of the simulation results on the x-y plane clearly shows the variation
characteristics of the along the shore. When $t = 0$, the shoreline was a straight line, and the channel was
in the middle of the shoreline. As time went on, the river mouth continued to move forward. From 0 to
230 2 Ma, the channel first swung to the north, then to the south, and shoreline began to bulge slightly
towards the sea side. From 2Ma, the channel continued to swing southward, until the time approached
4Ma and the river mouth began to turn north slowly. From 4Ma to 6Ma, the channel continued to swing
northward, and the convex part towards the sea side became more and more obvious. From 6Ma to
8Ma, the channel continued the previous trend, while the convex shoreline became asymmetry (an
235 increasing skewness to the north). From 8 Ma to 10 Ma, the principal line of the channel moved
southward, and the convex shoreline gradually returned to symmetry (Fig.7).

The simulation results also show some interesting features on longitudinal sections. Two sections
($y = 75\text{m}$ and $y = 125\text{m}$) perpendicular to the shoreline direction are selected (see Fig.7f for the
position of the section line). The two sections are located on the north and south sides of the main
240 channel. The distance between the channel and the two sections is varying. In the southern profile ($y =$
 75m), from 4 Ma to 10 Ma, the isochronous lines of the formation changes from sparse to dense, and
then from dense to sparse (i.e., the thickness of a single clinoform changes from thick to thin first and
then from thin to thick) (Fig.8). This is completely contrary to that observed in the northern profile ($y =$
 125m). From 4Ma to 10Ma, the isochronous lines first changes from dense to sparse, and then from



245 sparse to dense, reflecting that the deposition rate first increases and then decreases (Fig.9).

Under the parameters shown in Tab. 1, due to the existence of estuaries, shoreline will bulge towards the sea side. A closer distance to the river mouth could result in a higher sedimentation rate and a greater shoreline advancing speed. From 2 Ma, the convex shape of the shoreline towards the sea side became more and more apparent, similar to the morphology of some real-world Deltas (Fig.10).

250 2) Model 2

This code can be applied not only to marginal marine environments but also to the continental fault basins. Taking the 3 + 4 sand groups of the third member of Shahejie Formation in the Gaobei slope belt of Nanpu Sag in Bohai Bay Basin as an example, we conducted a simplified 2D real case study. The basic geological background is as follows: During the deposition period of this set of strata, 255 the normal fault tectonic movement in the north of the sag was active, which was the main controlling factor leading to the increase of accommodation space. At the same time, the terrigenous clasts came from the north is sufficient, and the basin was in a balanced state (Li et al., 2018). According to the geological background, a simplified reconstruction model (Model 2) was designed, which assumed that the subsidence rate of the boundary fault and sediment supply rate is constant, neglected the effect of 260 isostasy, and considered the effect of sediment compaction.

The simulation results are shown in Fig.11. From the perspective of temporal and spatial stratigraphy, the shoreline mainly moved towards the sag center during the early stage, and then moved back to the land side. The deepest water depth occurs in the middle south part at 2 Ma (Fig.11a). This shoreline phenomenon is usually called autoretreat (Muto and Steel, 2002). The sand fraction section 265 shows that the steep slope belt in the north is richer in sand content than the south (Fig.11b). The porosity section shows that the porosity generally decreases from bottom to top. The porosity also varies horizontally, especially when the depth is deeper than 800 m. The porosity in the north is larger than that in the south.

Due to the over-simplified assumptions, the simulation results are not necessarily be consistent 270 with every practical borehole. However, the general trends are revealed through the simulation, which can strengthen or improve our existing understanding and guide us to seize the main direction. Also, the facies simulation results were in good agreement with the Sedpak results used in Li et al., 2018.



5 Discussion

Sedapp is a diffusion-based model, and its transport coefficient is a function of both distance
275 from estuary and water depth. Compared with most existing diffusion models based only on water
depth, this modification has great advantages in fluvial-deltaic environments, especially for 3D
scenarios. Sedapp not only simulates some surface landscapes, but it also reveals some interesting
internal features. In the sections beside the channel in Model 1, the formation rate of the clinoforms has
close relationship with the distance between the channel and the section. This may be of great
280 significance to the analysis of ancient strata. Considering the resolution of seismic data, it is easier to
observe the changes in the density of the foreset than to directly find a channel. This may provide some
important supplementary information in areas with less borehole data.

Sedapp also showed strong simulation ability in 2D scenarios. It is not only competent for the
shallow sea environment of continental margin, but also competent for the simulation of continental
285 fault basin (Fig.11). The simulation results have strong comparability with previous studies (Li et al.,
2018). In addition, Sedapp can avoid some potential problems that the water depth models may meet.
The simulation results of Sedapp and water depth models are not very different where the original slope
is gentle (Fig.12a, Fig.12b). However, when the slope is steep, the differences are obvious: due to the
steep slope and the sharp increase of water depth, the slope break trajectory simulated by the water
290 depth based model increases significantly, even if the sea level remains unchanged at 6m (Fig.12c).
This is seriously contrary to the common sense, especially in estuary or delta front environments. In
contrast, Sedapp does not face such a problem. As long as the sea level is constant, the slope break line
will remain in a straight line and the clinoforms will also move smoothly to the ocean (Fig.12d).

The transport coefficient is a relatively long-term geomorphologic physical quantity, while wave,
295 tidal, and current energy are relatively short-term hydrodynamic quantities. However, they are closely
related. A river entering the sea is a type of jet flow phenomenon. The flow velocity decreases rapidly
from the river mouth to the sea, which also has a strong negative correlation with the distance to the
mouth of the river. The contour map of water flow velocity is fan-shaped. At the same time, the
decrease of velocity is also an important cause of sediment deposition, which also explains the close
300 fan-shaped morphology of a delta front. Correspondingly, an increase in water depth will also decrease
the flow velocity. For the open coast without river injection, a model based on water depth seems to be



reasonable. However, for a coast with river injection, it is difficult to explain the formation of the fan-shaped morphology of a delta. Therefore, it can be concluded that, in more general cases, the transport coefficient should be a function of short-term water energy, which is related to both the estuary distance and the water depth. When there is river injection, the river process is dominant and the estuary distance function is a reasonable proxy for the transport coefficient. When there is no river injection, the water depth plays the main role. In addition, the particle size is also one of the decisive factors (Nash 1980; Andrews and Bucknam 1987). Hence, a choice function (see Eq. (9)) and differentiated α 's are used to adapt different environments and lithologies. Although the current results of Sedapp seem plausible, these settings for transport coefficient are still empirical. Due to the complex nature of the transformation from short-term processes to long-term ones, it is difficult to build an accurate bridge between sediment hydrodynamics and stratigraphic formation, while it may be the focus of the next step.

6 Code availability

The current version of model is available from the project website: <http://zenodo.org/record/4133262> under the [Creative Commons Attribution 4.0 International License](#). The exact version of the model used to produce the results used in this paper is archived on Zenodo. Input data and scripts of the case studies are also presented in this site. For more details about Sedapp, please contact Jingzhe Li via email lijingzhe@qust.edu.cn.

Contribution of each author

JL developed the main algorithm of Sedapp and took the lead in writing the manuscript. PL developed the FVM solver for Sedapp. PL, SS, ZS, YZ, LG, JZ and DD participated in the conceiving of the presented idea. SS supervised the project.

Acknowledgement

Financial support was provided by the Initial Fund for Young Scholars of Qingdao University of Science and Technology, National Natural Science Foundation of China (42002169) and the Research Funding from King Abdullah University of Science and Technology (KAUST) through the grants



BAS/1/1351-01. Jingfa Li from Beijing Institute of Petrochemical Technology, Jie Chen from Xi'an Jiaotong University and Hua Zhong from Guangdong University of Finance and Economics also
330 offered constrictive advices.



Reference

- Andrews DJ, Bucknam RC. Fitting degradation of shoreline scarps by a nonlinear diffusion model. *Journal of Geophysical Research: Solid Earth*. 1987 Nov 10;92(B12):12857-67.
- 335 Athy, Lawrence Ferdinand. "Density, porosity, and compaction of sedimentary rocks." *Aapg Bulletin* 14, no. 1 (1930): 1-24.
- Burgess PM, Lammers H, van Oosterhout C, Granjeon D. Multivariate sequence stratigraphy: Tackling complexity and uncertainty with stratigraphic forward modeling, multiple scenarios, and conditional frequency maps. *AAPG bulletin*. 2006 Dec 1;90(12):1883-901.
- 340 Burgess PM, Prince GD. Non - unique stratal geometries: implications for sequence stratigraphic interpretations. *Basin Research*. 2015 May 5;27(3):351-65.
- Burgess PM. A brief review of developments in stratigraphic forward modelling, 2000 - 2009.in: D.G. Roberts and A.W. Bally (Eds.) *Regional Geology and Tectonics: Principles of Geologic Analysis*, Elsevier, 2012, Pages 94-111
- 345 Catuneanu O. Model-independent sequence stratigraphy. *Earth-science reviews*. 2019 Jan 1;188:312-88.
- Clarke TL, Swift DJ, Young RA. A stochastic modeling approach to the fine sediment budget of the New York Bight. *Journal of Geophysical Research: Oceans*. 1983 Nov 20;88(C14):9653-60.
- Dalman RA, Weltje GJ. SimClast: An aggregated forward stratigraphic model of continental
350 shelves. *Computers & geosciences*. 2012 Jan 1;38(1):115-26.
- Ding X, Salles T, Flament N, et al. Quantitative stratigraphic analysis in a source-to-sink numerical framework[J]. *Geoscientific Model Development*, 2019, 12(6).
- Fernandes, Nelson F., and William E. Dietrich. "Hillslope evolution by diffusive processes: The timescale for equilibrium adjustments." *Water Resources Research* 33, no. 6 (1997): 1307-1318.
- 355 Galy, Albert, and Christian France-Lanord. "Higher erosion rates in the Himalaya: Geochemical constraints on riverine fluxes." *Geology* 29, no. 1 (2001): 23-26.
- Granjeon D, Joseph P. Concepts and applications of a 3-D multiple lithology, diffusive model in stratigraphic modeling.
- Griffiths CM, Hadler-Jacobsen F. Practical dynamic modelling of clastic basin fill. In *Norwegian Petroleum Society Special Publications* 1995 Jan 1 (Vol. 5, pp. 31-49). Elsevier.
- 360 Haq BU, Hardenbol JA, Vail PR. Chronology of fluctuating sea levels since the Triassic. *Science*. 1987 Mar 6;235(4793):1156-67.
- Hutton EW, Syvitski JP. Sedflux 2.0: An advanced process-response model that generates three-dimensional stratigraphy. *Computers & Geosciences*. 2008 Oct 1;34(10):1319-37.
- 365 Kaufman P, Grotzinger JP, McCormick DS, Franseen EK, Watney WL. Depth-dependent diffusion algorithm for simulation of sedimentation in shallow marine depositional systems. In *Sedimentary Modeling: Computer Simulations and Methods for Improved Parameter Definition 1991* (Vol. 233, pp. 489-508). Kansas Geological Survey Bulletin.
- Kendall CS, Strobel J, Cannon R, Bezdek J, Biswas G. The simulation of the sedimentary fill of
370 basins. *Journal of Geophysical Research: Solid Earth*. 1991 Apr 10;96(B4):6911-29.
- Kevin Ushey, JJ Allaire, Hadley Wickham and Gary Ritchie (2020). *rstudioapi: Safely Access the RStudio API*. R package version 0.11. <https://CRAN.R-project.org/package=rstudioapi>
- Lawrence DT, Doyle M, Aigner T. Stratigraphic simulation of sedimentary basins: concepts and calibration. *Aapg Bulletin*. 1990 Mar 1;74(3):273-95.
- 375 Li J, Liu P, Zhang J, Sun S, Sun Z, Du D, Zhang M. Base Level Changes based on Basin Filling



- Modelling: a Case Study from the Paleocene Lishui Sag, East China Sea Basin. *Petroleum Science*. <https://doi.org/10.1007/s12182-020-00478-2>
- Li J, Liu S, Zhang J, Fan Z, Sun Z, Zhang M, Yuan Y, Zhang P. Architecture and facies model in a non-marine to shallow-marine setting with continuous base-level rise: An example from the Cretaceous Denglouku Formation in the Changling Depression, Songliao Basin, China. *Marine and Petroleum Geology*. 2015 Dec 1;68:381-93.
- Li J, Zhang J, Sun S, Zhang K, Du D, Sun Z, Wang Y, Liu L, Wang G. Sedimentology and mechanism of a lacustrine syn-rift fan delta system: A case study of the Paleogene Gaobei Slope Belt, Bohai Bay Basin, China. *Marine and Petroleum Geology*. 2018 Dec 1;98:477-90.
- "Liu P, Yao J, Couples G D, et al. Numerical modelling and analysis of reactive flow and wormhole formation in fractured carbonate rocks. *Chemical Engineering Science*, 2017, 172: 143-157.
- Matthew Strimas-Mackey (2020). smoothr: Smooth and Tidy Spatial Features. R package version 0.1.2. <https://CRAN.R-project.org/package=smoothr>
- Moukalled F, Mangani L, Darwish M. *The finite volume method in computational fluid dynamics*. Berlin, Germany:: Springer; 2016.
- Muto T, Steel RJ. Role of autoretreat and A/S changes in the understanding of deltaic shoreline trajectory: a semi - quantitative approach. *Basin Research*. 2002 Sep 1;14(3):303-18.
- Nash DB. Morphologic dating of degraded normal fault scarps. *The Journal of Geology*. 1980 May 1;88(3):353-60.
- Paola C. Quantitative models of sedimentary basin filling. *Sedimentology*. 2000 Feb;47:121-78.
- Pelletier, Jon. "Fundamental Principles and Techniques of Landscape Evolution Modeling." In *Treatise on Geomorphology*, pp. 29-43. Elsevier Inc., 2013.
- R Core Team (2020). *R: A language and environment for statistical computing*. R Foundation for Statistical Computing, Vienna, Austria. URL <https://www.R-project.org/>.
- Ramos V, Carballo R, Ringwood JV. Application of the actuator disc theory of Delft3D-FLOW to model far-field hydrodynamic impacts of tidal turbines. *Renewable energy*. 2019 Aug 1;139:1320-35.
- Rivenaes JC. Application of a dual - lithology, depth - dependent diffusion equation in stratigraphic simulation. *Basin Research*. 1992 Jun 1;4(2):133-46.
- Rivenaes JC. Impact of sediment transport efficiency on large - scale sequence architecture: results from stratigraphic computer simulation. *Basin Research*. 1997 Jun;9(2):91-105.
- Sacchi Q, Borello ES, Weltje GJ, Dalman R. Increasing the predictive power of geostatistical reservoir models by integration of geological constraints from stratigraphic forward modeling. *Marine and Petroleum Geology*. 2016 Jan 1;69:112-26.
- Sacchi Q, Weltje GJ, Verga F. Towards process-based geological reservoir modelling: Obtaining basin-scale constraints from seismic and well data. *Marine and Petroleum Geology*. 2015 Mar 1;61:56-68.
- Salles T, Ding X, Brocard G. pyBadlands: A framework to simulate sediment transport, landscape dynamics and basin stratigraphic evolution through space and time[J]. *PloS one*, 2018, 13(4): e0195557.
- Sangster C, Piper DJ, Hawie N, Pe - Piper G, Saint - Ange F. Forward stratigraphic modelling of sediment pathways and depocentres in salt - influenced passive - margin basins: Lower Cretaceous, central Scotian Basin. *Basin Research*. 2019 Jul 14;31(4):728-53.
- Slater JG, Christie PA. Continental stretching: An explanation of the post - mid - Cretaceous subsidence of the central North Sea basin. *Journal of Geophysical Research: Solid Earth*. 1980 Jul



- 420 10;85(B7):3711-39.
Strobel J, Cannon R, Christopher GS, Kendall CS, Biswas G, Bezdek J. Interactive (SEDPAK) simulation of clastic and carbonate sediments in shelf to basin settings. *Computers & Geosciences*. 1989 Jan 1;15(8):1279-90.
- Syvitski JP, Hutton EW. 2d sedflux 1.0 c:: an advanced process-response numerical model for the
425 fill of marine sedimentary basins. *Computers & Geosciences*. 2001 Jul 1;27(6):731-53.
- Versteeg HK, Malalasekera W. An introduction to computational fluid dynamics: the finite volume method. Pearson education; 2007.
- Yuan XP, Braun J, Guerit L, Simon B, Bovy B, Rouby D, Robin C, Jiao R. Linking continental
430 erosion to marine sediment transport and deposition: A new implicit and O (N) method for inverse analysis. *Earth and Planetary Science Letters*. 2019 Oct 15;524:115728.
- Zhang J, Sylvester Z, Covault J. How do basin margins record long-term tectonic and climatic changes?[J]. *Geology*, 2020.
- Zhu Z, LeRoy JZ, Rhoads BL, García MH. HydroSedFoam: A new parallelized two-dimensional
435 hydrodynamic, sediment transport, and bed morphology model. *Computers & geosciences*. 2018 Nov 1;120:32-9.

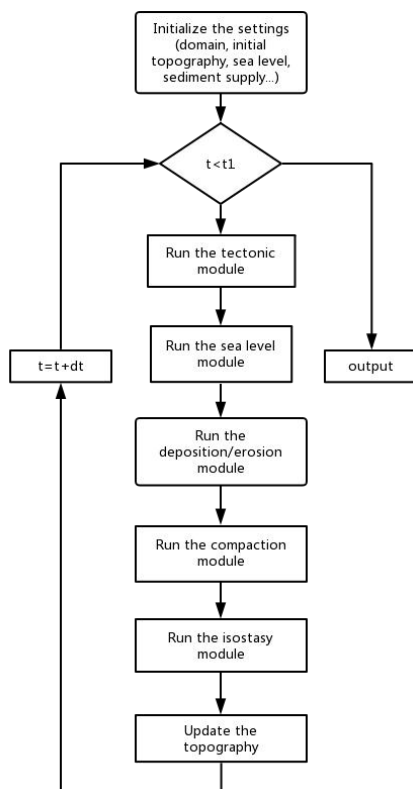
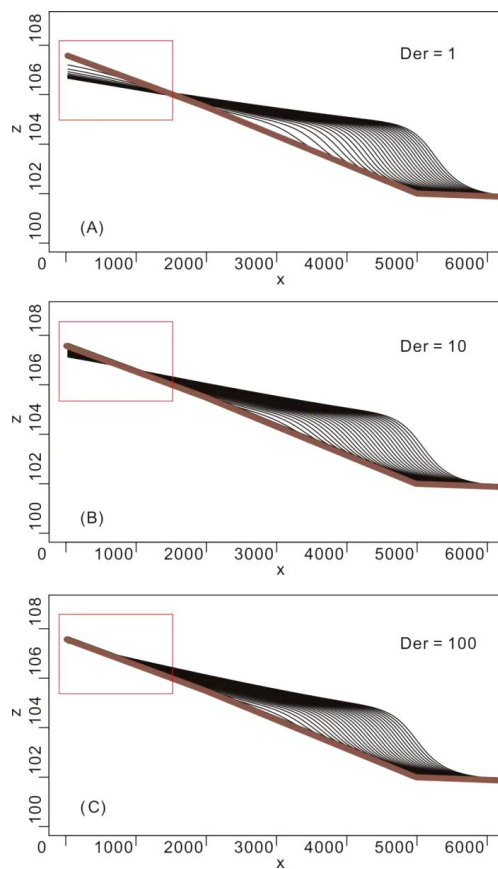


Fig. 1 Flowchart of the algorithms in Sedapp



440 Fig. 2 Dip direction section with different Der values (Der = 1, Der = 10, Der = 100 respectively).

Erosion will be switched off if Der is large enough.

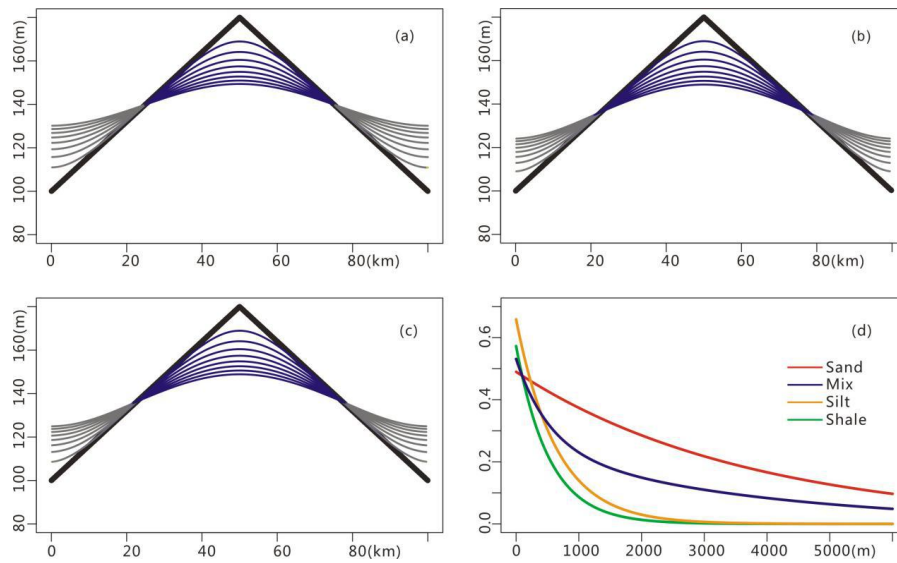


Fig. 3 Customized compaction and the porosity curves. a) the x-z plot with original
depth-porosity scale; b) the x-z plot with magnified depth-porosity scale (x100) to enhance compaction;
445 c) the x-z plot with magnified depth-porosity scale (x1000) to enhance compaction; d) Depth-porosity
curves used in the compaction module (the mix indicates mixed 50%-50% sand and shale. Details see
Athy, 1930; Sclater and Christie 1980)

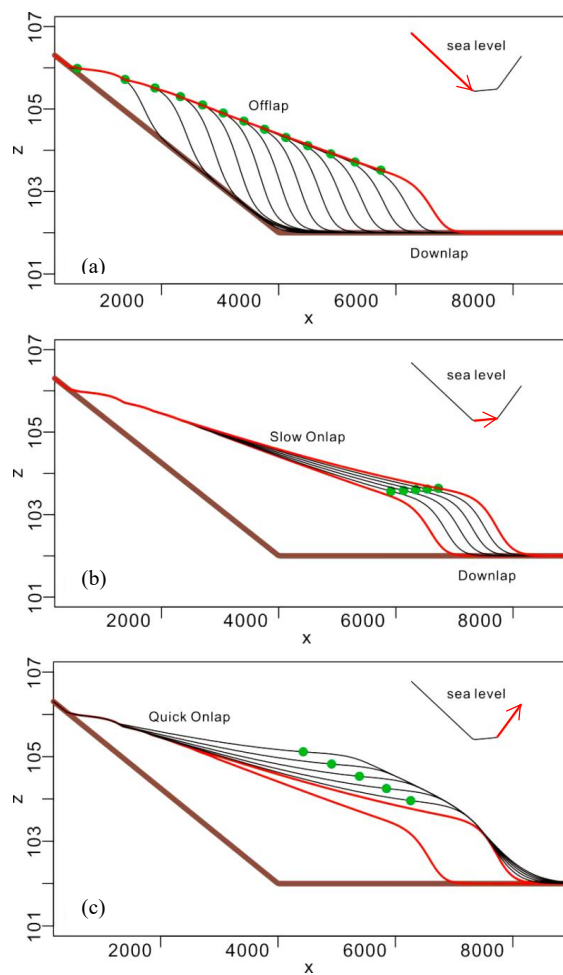
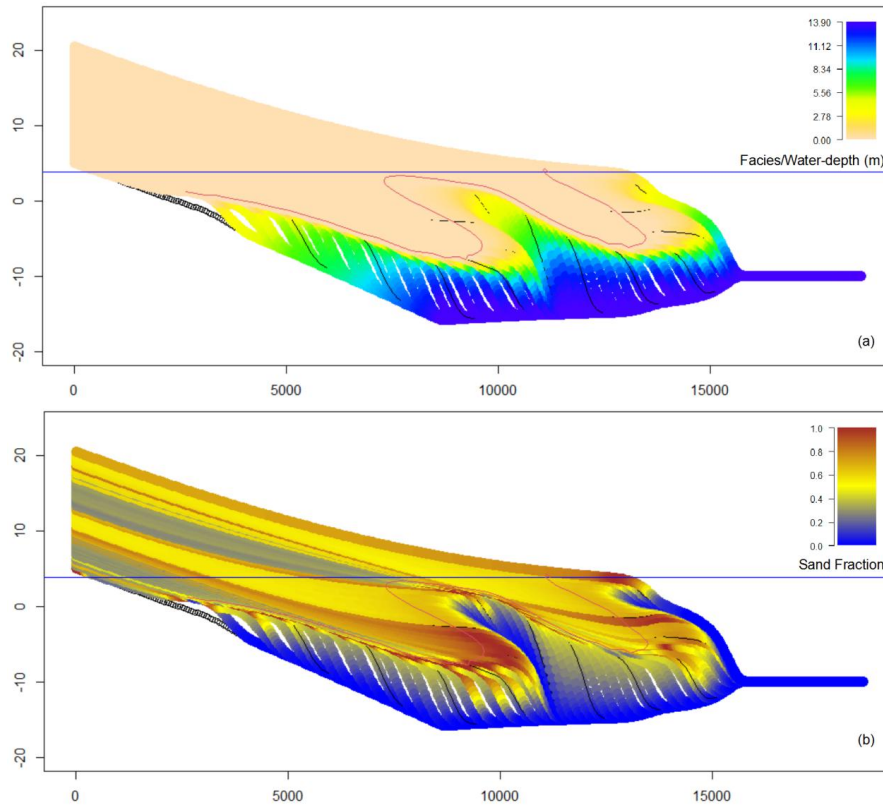
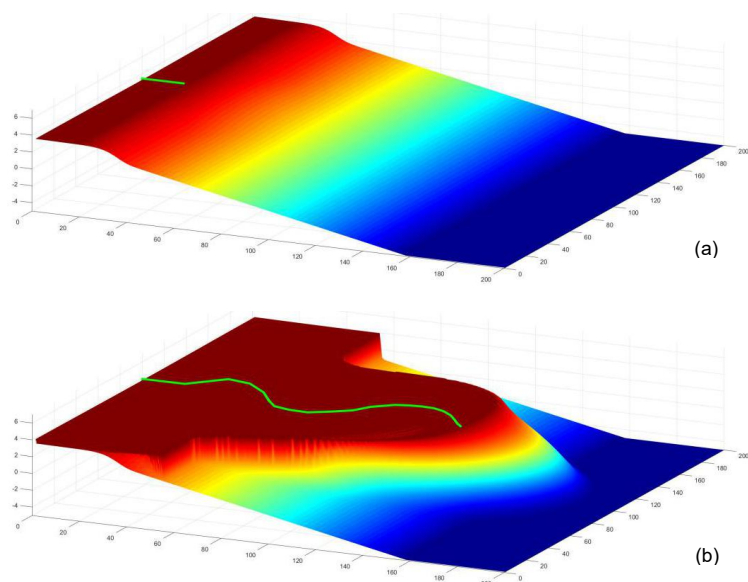


Fig. 4 Typical stacking patterns acquired through different sea level change rates



450

Fig. 5 Simulated stratigraphy under two full sea level cycles. A) facies section and B) lithological section.



455

Fig. 6 The initial topography and the simulated results of Model 1. (a): the initial topography; (b): the topography at $t=10$ Ma.

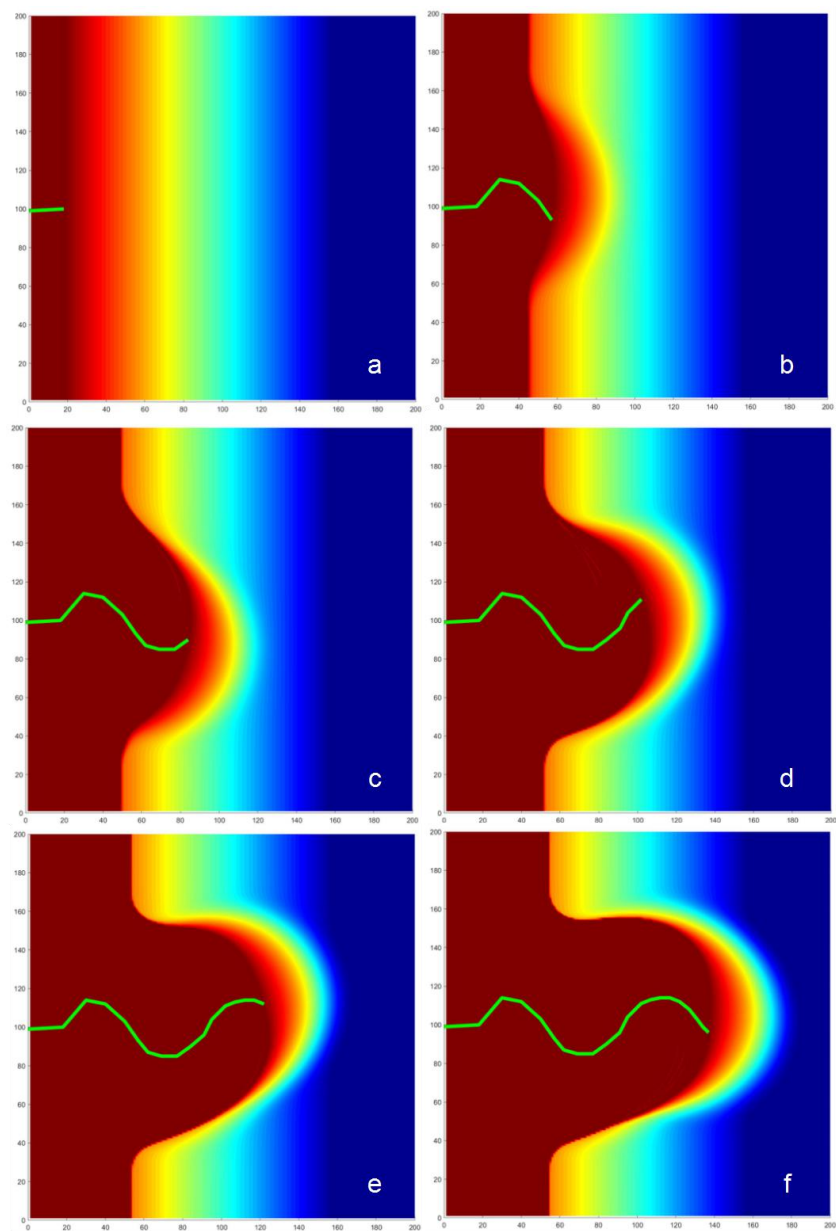


Fig. 7 Plane view of Model 1 results. (a): $t=0$ Ma; (b): $t=2$ Ma; (c): $t=4$ Ma; (d) $t=6$ Ma; (e) $t=8$ Ma; (f) $t=10$ Ma.

460

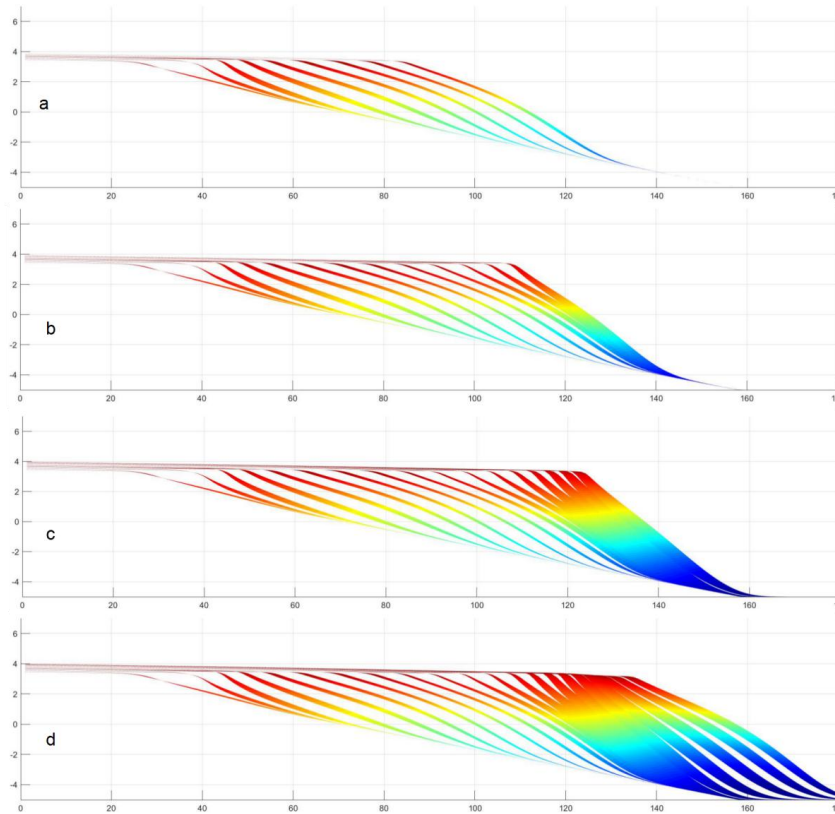


Fig. 8 Cross section at $x=75m$. (a): $t=4Ma$; (b): $t=6 Ma$; (c): $t=8Ma$; (d) $t=10Ma$.

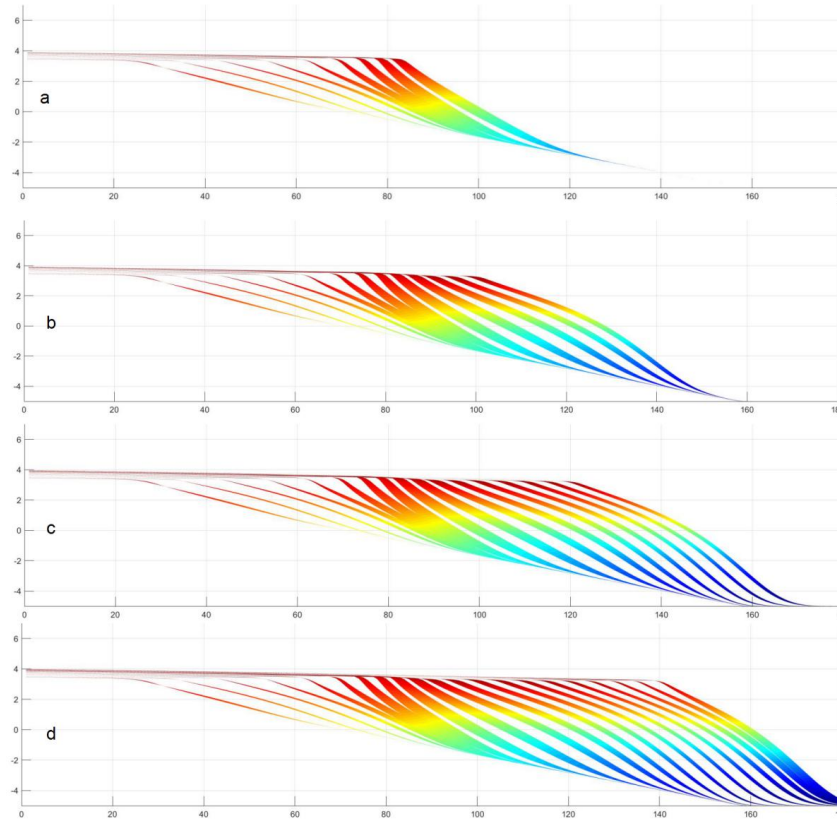


Fig. 9 Cross section at $x=125\text{m}$. (a): $t=4\text{Ma}$; (b): $t=6\text{Ma}$; (c): $t=8\text{Ma}$; (d) $t=10\text{Ma}$.

465

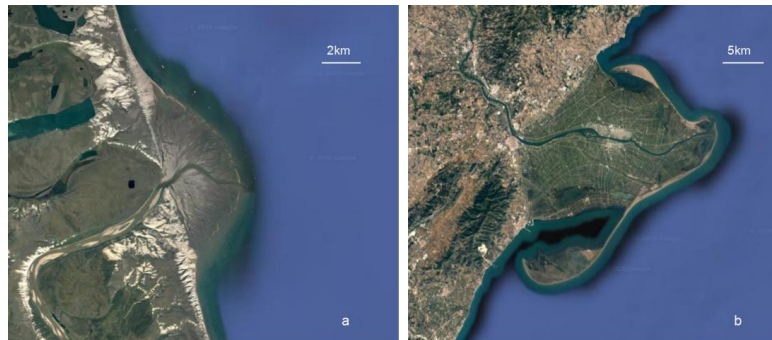
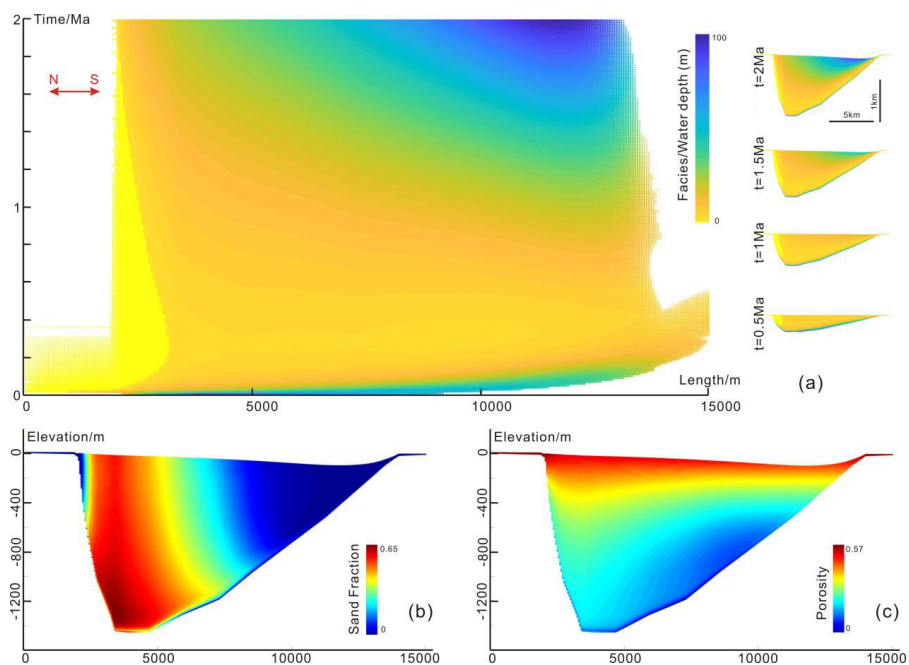
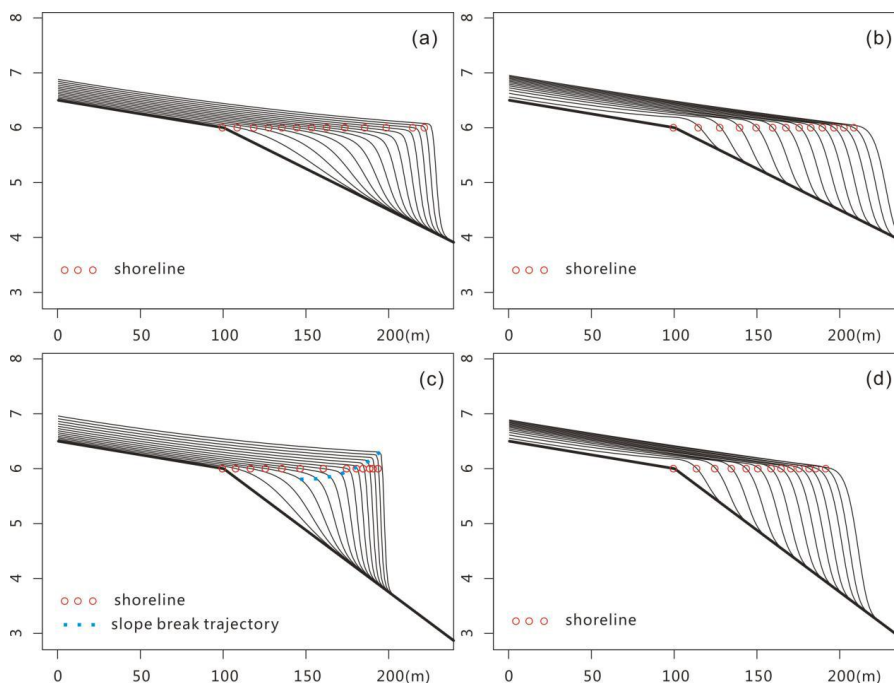


Fig. 10 Horton River Delta in Canada (a) and Ebro Delta in Mediterranean Sea (b) (taken from © Google Maps)



470 Fig. 11 Simulation results of Gaobei Slope Belt during the study interval. a) Sedapp results of facies in the time domain (Wheeler diagram) and depth domain at different times; b) Sedapp results of sand fraction in the depth domain. c) Sedapp results of porosity in the depth domain



475 Fig. 12 The differences between two algorithms. a) Clinoforms of gentle slope created in water depth models; b) Clinoforms of gentle slope created in Sedapp; a) Clinoforms of steep slope created in water depth models; b) Clinoforms of steep slope created in Sedapp.

Tab. 1 Main simulation parameters of Model1 (see 2.1 above for meanings of the notations)

Parameter	Value
α	1000
β	500
η	2
α_{wd}	10000
β_{wd}	0.16
η_{wd}	1
ε	0
<i>Der</i>	1

480